Semiconductor Physics, Quantum Electronics & Optoelectronics, 2026. V. 29, No 3. P. 332-335.

Semiconductor physics

EPR properties of $MnGaInS_4$ single crystal

N.N. Niftiyev

Azerbaijan State Pedagogical University, Az-1000 Baku, Azerbaijan
E-mail: niftiyevnamiq7@gmail.com

Abstract. The EPR properties of $MnGaInS_4$ single crystal were investigated within the temperature range 5.6...103 K. At low temperatures (5.6 K), the crystal is in the antiferromagnetic phase; the line is broad ($\Delta H \approx 234$ G) and Gaussian in shape. With increasing the temperature, the line narrows and becomes Lorentzian in shape, which indicates an increase in spin-lattice interactions. The temperature dependence of the resonance line width is explained by the Kubo–Anderson model; the relaxation time τ is short at low temperatures ($\tau \approx 2.4 \cdot 10^{-10}$ s) and long at high temperatures. With increasing the temperature, the *g*-factor increases from 1.99 to 2.00, due to the thermal expansion of the crystal lattice and the strengthening of spin-orbit interactions. The intensity of the EPR signal increases with increasing the temperature because, as the temperature increases, more spin centers participate in the resonance process by overcoming the energy barrier. Thus, temperature-dependent magnetic phase transitions, spin dynamics, and *g*-factor variation in $MnGaInS_4$ single crystal have been clearly identified. These results indicate the material potential for future magnetic and spintronic applications.

Keywords: $MnGaInS_4$, EPR, *g*-factor, resonance linewidth, relaxation time.

https://doi.org/10.15407/spqeo29.03.332
PACS 75.40.Gb, 75.50.Ee, 76.30.-v

Manuscript received 06.11.25; revised version received 03.08.26; accepted for publication 16.09.26; published online 25.09.26.

1. Introduction

Recently, AB_2X_2-type chalcogenide compounds (where A – Mn, Fe, Co, Ni; B – Ga, In; X – S, Se, Te) belonging to the class of multicomponent semiconductors have attracted great scientific interest due to their unique physical properties and wide application potential [1–23]. These types of materials are rich in both the magnetic properties of transition metal ions and the highly anisotropic electronic structures of chalcogens. These types of compounds are considered promising for the creation of lasers, light modulators, photodetectors, and other functional devices controlled by a magnetic field [1–10]. Interest in these compounds has increased significantly in the last decade. This is associated with the emergence of two-dimensional materials that hold great promise for spintronics applications and open a new path that can significantly advance the development of electronics and information technologies [11, 12]. According to the results of several studies, these compounds are also promising for use in renewable energy sources, since they exhibit tunable electronic, optical, and magnetic properties [13, 14]. The potential of using heterojunctions formed from some of the above-mentioned compounds and photocatalytic water splitting in solar cells has also been demonstrated [15]. In addition, some studies [16–18] have shown that MIn_2S_4-type compounds (M = Mn, Fe, Co) have a spinel structure, and their nanocomposites with carbon nanotubes are highly promising as a new class of anode materials for stable ion storage in Li and Na ion batteries. Based on $FeIn_2Se_4$ crystals, heterojunctions have been prepared [19], and the $FeIn_2S_4$ compound has been synthesized in the form of nanocrystals [20]. In [21, 22], new layered semiconducting compounds containing $MnGaInS_4$ were synthesized, and their crystal structure was studied. In this work, we focus on electron paramagnetic resonance spectra to further investigate the magnetic behavior and spin dynamics of $MnGaInS_4$ single crystals.

2. Experimental method

$MnGaInS_4$ single crystals were obtained by the Bridgman method. X-ray diffraction showed that they crystallize in a single-pack polytype $ZnIn_2S_4$ structure with crystal lattice parameters $a = 3.81$, $c = 12.17$ Å, $z = 1$ ($P3m1$ space group) [22]. EPR spectra were recorded using a Varian spectrometer operating at a microwave frequency of 9.47 GHz and a magnetic field modulation frequency of 100 kHz. Measurements were conducted on single-crystal samples within a temperature range of 5.6 to 103 K. Precise orientation of the crystals relative to the applied magnetic field (H‖[001]) was achieved using a goniometer. The first derivative of the EPR absorption signal was captured, with the absorbed energy directly proportional to the total number of unpaired electrons in the sample. The resonance linewidth (ΔH) was determined

by measuring the distance between the magnetic field values corresponding to the minimum and maximum of the first derivative of the absorption line.

3. Result and discussions

Fig. 1 shows the EPR spectra of a single crystal of $MnGaInS_4$ at various temperatures. It is known that the $MnGaInS_4$ compound is considered as a mixture of the $MnGa_2S_4$ and $MnIn_2S_4$ systems. Here, Ga^{3+} ions have a smaller radius and a strong ligand field, which increases the Neel temperature (T_N) by enhancing the spin-spin interaction, while In^{3+} ions, on the contrary, have a larger radius and a weak ligand field, which reduces T_N. For the α-modification of the $MnGa_2S_4$ compound, $T_N \approx 11$ K, for the β-modification, $T_N \approx 23.5$ K [23], and for $MnIn_2S_4$, $T_N = 4.9$ K [24]. Therefore, the Neel temperature of the $MnGaInS_4$ compound lies between these values and is estimated to be approximately 10–15 K. Thus, at low temperatures, the crystal is in an antiferromagnetic phase, where the spins are arranged in long-range order, creating strong spin-spin interactions. These interactions lead to a wide spectrum of local magnetic fields, and as a result, inhomogeneous broadening becomes dominant. Since each spin center experiences a different local field, the line morphology becomes Gaussian. These inhomogeneous local fields and the "frozen" spin state create conditions for line broadening. The broad ($\Delta H \approx 234$ G) and Gaussian-shaped EPR signal observed at 5.6 K is considered a characteristic feature of antiferromagnetic ordering [25].

With increasing the temperature (at 36 and 103 K), thermal fluctuations in the crystal become stronger, the spins behave more freely, and the antiferromagnetic ordering is disrupted, passing into the paramagnetic phase. Under these conditions, since the local field differences decrease, homogeneous relaxation mechanisms prevail, and as a result, the line takes on a Lorentzian shape. A Lorentzian-shaped line represents homogeneous broadening and is characteristic of the paramagnetic phase [25].

Fig. 2 shows the temperature dependence of the resonance line width ΔH. Increasing the temperature from 5.6 to 103 K causes the line to narrow.

At low temperatures, local magnetic field inhomogeneities (spin-spin interactions, crystal field anisotropy) broaden the line. With increasing the temperature, relaxational motions (ion drift, phonon vibrations) intensify, local field fluctuations change more rapidly, and as a result, the line becomes homogeneous and narrows. This mechanism is explained according to the Kubo–Anderson fluctuation model [25]. The line width ΔH is determined by both spin-spin (τ_2-based, inhomogeneous width) and spin-lattice (τ_1-based, homogeneous width) relaxation processes [25]:

$$\Delta H = \frac{1}{\tau_2} + \frac{1}{\tau_1}.$$

In the paramagnetic and antiferromagnetic phases, the dominant relaxation mechanisms differ. In the antiferromagnetic phase, ΔH is primarily governed by spin-lattice relaxation because spin energy levels interact

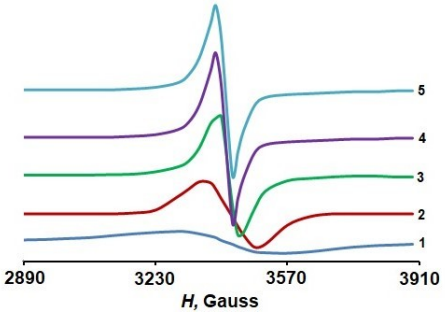

Fig. 1. EPR spectrum of $MnGaInS_4$ single crystals at temperatures T, K: *1* – 5.6, *2* – 20, *3* – 36, *4* – 70, *5* – 103.

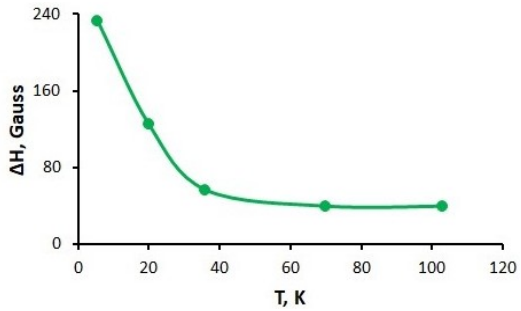

Fig. 2. Temperature dependence of the width of the resonance line for $MnGaInS_4$ single crystals.

with lattice phonons. In the paramagnetic phase, however, ΔH depends mainly on spin-spin relaxation, since at higher temperatures, spin interactions weaken and phonon-induced fluctuations homogenize the line. Thus, although ΔH remains inversely proportional to the relaxation time ($\Delta H \propto 1/\tau$), the dominant mechanism varies between the two phases.

With increasing the temperature, the spin-lattice component becomes stronger, the role of spin-spin interactions decreases, and the line becomes narrower. At low temperatures (5.6 K), in the antiferromagnetic case, ΔH is maximized due to the strong spin-spin interactions. As the temperature increases, the spins interact less, resulting in the line narrowing.

The g-factor for the $MnGaInS_4$ crystal was calculated using the expression

$$g = \frac{h\nu}{\mu_B H_r}.$$

Here, h is the Planck constant, ν is the microwave frequency of the EPR spectrometer (~9.5 GHz), μ_B is the Bohr magneton, and H_r is the resonance value of the magnetic intensity. With increasing the temperature, the g-factor increases from 1.99 to 2.00. This change is explained by the thermal expansion of the crystal lattice, the strengthening of spin-orbit interactions, and the modulation of local anisotropy with temperature. In the antiferromagnetic phase (5.6 K), the rigid order of the spins causes g to remain stable, but with increasing the temperature, the spins become free in the paramagnetic phase, and the structural anisotropy becomes fully expressed, which leads to a small but significant increase in g.

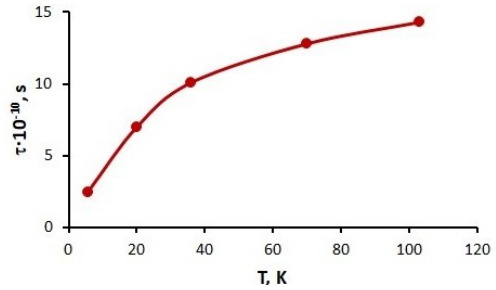

Fig. 3. Temperature dependence of the relaxation time for $MnGaInS_4$ single crystals.

The relaxation time is determined by the following formula:

$$\tau = \frac{\eta}{g\mu_B \Delta H}.$$

At 5.6 K, $\tau = 1.054\cdot10^{-34}$ J·s/[$1.99\cdot9.274\cdot10^{-24}$ $J/T\times$ $\times2.34\cdot10^{-2}$] ≈ $2.4\cdot10^{-10}$ s. The relaxation time is ~10^{-10} s. As shown in Fig. 3, the relaxation time increases with increasing temperature. This is explained by the higher mobility of spins under thermal influence and faster adaptation to local field fluctuations due to phonon participation. At lower temperatures (antiferromagnetic phase), however, the relaxation becomes shorter due to strong spin interactions, which is also observed by the broad EPR line.

The intensity of the resonance curves is determined as follows [25]:

$$I = Y_{max}(\Delta H_{max})^2,$$

where $2Y_{max}$ corresponds to the signal amplitude scaled to the distance between the extrema on the line curve. The peak intensity term $2Y_{max}$ can be used as a parameter of the signal intensity only for comparing lines of the same width. ΔH_{max} is the distance between the extrema of the first derivative of the signal. It has been found that the EPR intensity increases with increasing temperature. This behavior is explained by the model of thermally activated magnetic centers: as the temperature increases, more spin centers overcome the energy barrier and participate in the resonance process [25]. The EPR intensity expresses the magnitude of the signal at resonance and depends on the number of magnetic centers in the spin system, the response of these centers to the magnetic field, and their relaxation times. With increasing the temperature, the magnetic centers become more active. The number of spins that overcome the energy barrier and enter the resonance condition increases. This leads to an increase in the EPR intensity [25].

4. Conclusions

As a result of the conducted research, the EPR properties of the $MnGaInS_4$ single crystal within the temperature range from 5.6 to 103 K were investigated. At low temperatures (5.6 K), the crystal is in the antiferromagnetic phase; the EPR line is broad ($\Delta H \approx 234$ G) and Gaussian-shaped. With increasing the temperature, the ordering weakens, the line narrows, and a Lorentz-shaped spectrum is formed, indicating an increase in spin-lattice interactions. The temperature dependence of the resonance line width was explained by the Kubo–Anderson model; the broadening at low temperatures is associated with local field inhomogeneities, and the narrowing at high temperatures is associated with homogeneous relaxation mechanisms. The relaxation time τ is short at low temperatures (≈ $2.4\cdot10^{-10}$ s), and long at high temperatures. As the temperature increases, the *g*-factor increases from 1.99 to 2.00, which is due to the thermal expansion of the crystal lattice and strengthening of spin-orbit interactions. The temperature dependence of the EPR signal intensity is explained by the increase in thermally activated magnetic centers. Overall, the EPR results of the $MnGaInS_4$ single crystal show that the magnetic properties of the material change sharply with temperature, and that the spin dynamics and the stability of the *g*-factor can be observed in both the antiferromagnetic and paramagnetic phases. These results are important for future magnetic and spintronic applications of Mn-based sulfide compounds.

References

1. Guratinder K., Schmidt M., Walker H.C. *et al*. Magnetic correlations in the triangular antiferromagnet $FeGa_2S_4$. *Phys. Rev. B*. 2021. **104**. P. 064412. https://doi.org/10.1103/PhysRevB.104.064412.
2. Gainza J., Guinazu O.N., Cespedes E., Falcon H. *et al*. Tunable inversion degree of $MnIn_2S_4$ thiospinels prepared by high-pressure synthesis, and its implication in the optical and magnetic properties. *J. Alloys Compd.* 2023. **969**. Art. 172413. https://doi.org/10.1016/j.jallcom.2023.172413.
3. Niftiyev N.N., Mammadov F.M., Dashdemirov A.O. *et al*. Some optoelectronic properties of $FeGaInSe_4$ crystals under laser excitation. *SPQEO*. 2025. **28**. P. 33–36. https://doi.org/10.15407/spqeo28.01.033.
4. Wyzga P., Veremchuk I., Bobnar M. *et al*. Ternary MIn_2S_4 (M = Mn, Fe, Co, Ni) thiospinels – Crystal structure and thermoelectric properties. *Z. Anorg. Allg. Chem.* 2020. **646**. P. 1091–1098. https://doi.org/10.1002/zaac.202000014.
5. Niftiyev N.N., Dashdemirov A.O., Mammadov F.M., Muradov M.B. Frequency dispersion of dielectric coefficients of $MnGaInTe_4$ crystals. *SPQEO*. 2024. **27**. P. 189–193. https://doi.org/10.15407/spqeo27.02.189.
6. Niftiev N.N. Photoelectric properties of $MnIn_2S_4$ crystals. *J. Appl. Spectrosc.* 2022. **88**. P. 1234–1236. https://doi.org/10.1007/s10812-022-01304-w.
7. Yang J., Zhou J., Fang J., We H. Magnetic and transport properties of a ferromagnetic layered semiconductor $MnIn_2Se_4$. *Appl. Phys. Lett*. 2019. **115**. P. 222101. https://doi.org/10.1063/1.5126233.
8. Myoung B.R., Lim J.T., Kim C.S. Investigation of magnetic properties on spin-ordering effects of $FeGa_2S_4$ and $FeIn_2S_4$. *J. Magn. Magn. Mater*. 2017. **438**. P. 121–125. https://doi.org/10.1016/j.jmmm.2017.04.056.
9. Hwang Y., Choi J., Ha Y. *et al*. Electronic and optical properties of layered chalcogenide $FeIn_2Se_4$. *Curr. Appl. Phys*. 2020. **20**. P. 212–218. https://doi.org/10.1016/j.cap.2019.11.005.

10. Niftiev N.N. Optical absorption of $MnGa_2S_4$ single crystals. *Intermetallics.* 2003. **11**. P. 975–977. https://doi.org/10.1016/S0966-9795(03)00051-7.
11. Nakatsuji S., Tonomura H., Onuma K. *et al*. Spin disorder and order in quasi-2d triangular Heisenberg antiferromagnets: comparative study of $FeGa_2S_4$, $Fe_2Ga_2S_5$ and $NiGa_2S_4$. *Phys. Rev. Lett.* 2007. **99**. P. 157203. https://doi.org/10.1103/PhysRevLett.99.157203.
12. Takubo K., Mizokawa T., Nambu Y., Nakatsuji S. Electronic structure study of triangular lattices in $FeGa_2S_4$, $Fe_2Ga_2S_5$ and $NiGa_2S_4$: Photoemission spectroscopy and Hartree–Fock calculations. *Phys. Rev. B*. 2009. **79**. P. 134422. https://doi.org/10.1103/PhysRevB.79.134422.
13. Sharan A., Sajjad M., Singh D.J. *et al.* Two-dimensional ternary chalcogenides FeX_2Y_4 (X = Ga, In; Y = S, Se, Te): Promising materials for sustainable energy. *Phys. Rev. Mater*. 2022. **6**. P. 094005. https://doi.org/10.1103/PhysRevMaterials.6.094005.
14. Shan Y., Li T. Electronic reconfiguration induced by anchoring orbital interaction onto asymmetric $FeIn_2S_4$ surface for hydrogen evolution reaction. *Phys. B. Condens. Matter*. 2023. **654**. P. 414704. https://doi.org/10.1016/j.physb.2023.414704.
15. Song Y., Guoa Y., Qia Sh. *et al.* $Cu_7S_4/MnIn_2S_4$ heterojunction for efficient photocatalytic hydrogen generation. *J. Alloys Compd*. 2021. **884**. P. 161035. https://doi.org/10.1016/j.jallcom.2021.161035.
16. Yan D., Li K., Yan Y. *et al.* Cubic spinel XIn_2S_4 (X = Fe, Co, Mn): A new type of anode material for superfast and ultrastable Na-ion storage. *Adv. Energy Mater.* 2021. **11**. P. 2102137. https://doi.org/10.1002/aenm.202102137.
17. Wu P., Huang Ch., Hsieh Ch., Liu W. Synthesis and characterization of $MnIn_2S_4$/single-walled carbon nanotube composites as an anode material for lithium-ion batteries. *Nanomaterials.* 2024. **14**. P. 716. https://doi.org/10.3390/nano14080716.
18. Muruganantham R., Chen J.-A., Yang C.-C. Spinel phase $MnIn_2S_4$ enfolded with reduced graphene oxide as composite anode material for lithium-ion storage. *Mater. Today Sustain*. 2023. **21**. P. 100278. https://doi.org/10.1016/j.mtsust.2022.100278.
19. Kim H., Tiwari A., Hwang E. *et al*. $FeIn_2S_4$ nanocrystals: A ternary metal chalcogenide material for ambipolar field-effect transistors. *Adv. Sci.* 2018. **5**. P. 800068. https://doi.org/10.1002/advs.201800068.
20. Kushnir B.V., Kovalyuk Z.D., Katerynchuk V.M. *et al*. Layered crystals $FeIn_2Se_4$, In_4Se_3 and heterojunctions on their basis. *Funct. Mater.* 2017. **24**. P. 372–375. https://doi.org/10.15407/fm24.03.372.
21. Haeuseler H. $MnGaInS_4$ and $MnIn_2S_2Se_2$, two new compounds with $ZnIn_2S_4$ structure. *Naturwissenschaften*. 1986. **73**. P. 264. https://doi.org/10.1007/BF00367778.
22. Haeuseler H., Stork H.J. Materials with layered structures. Part 6. $MnGaInS_4$, Crystal structure and phase width in the system $MnS–Ga_2S_3–In_2S_3$. *J. Mater. Chem.* 1992. **2**. P. 145–147. https://doi.org/10.1039/JM9920200145.
23. Rimet R., Buder R., Schlenker C. *et al*. New antiferromagnetic properties of manganese gallium sulfides $MnGa_2S_4$-α and $MnGa_2S_4$-β. *Solid State Commun*. 1981. **3**. P. 693–697. https://doi.org/10.1016/0038-1098(81)91080-2.
24. Hsu C.-I., Steger John J., DeMeo E.A. *et al*. Magnetic susceptibility of $MnIn_2S_4$. *J. Solid State Chem.* 1975. **13**. P. 304–306. https://doi.org/10.1016/0022-4596(75)90142-5.
25. Weil J.A., Bolton J.R., Wertz J.E. *Electron Paramagnetic Resonance: Elementary Theory and Practical Applications.* Wiley, 2007.

Namig Niftiyev, Doctor of Sciences in Physics, Associate Professor of the General Physics Department of the Azerbaijan State Pedagogical University. He is the author of more than 140 scientific works, 1 monograph, and 3 textbooks. The area of his interests is the study of electrophysical and optical properties of complex semiconductor compounds and electronic and optical processes in them. https://orcid.org/0009-0002-0263-7956

ЕПР-властивості монокристала $MnGaInS_4$

N.N. Niftiyev

Анотація. Властивості ЕПР монокристала $MnGaInS_4$ досліджували в діапазоні температур 5,6–103 K. За низьких температур (5,6 K) кристал знаходиться в антиферомагнітній фазі, лінія широка ($\Delta H \approx 234$ G) та має гауссову форму. Зі збільшенням температури лінія звужується та набуває лоренцевої форми, що свідчить про збільшення спін-граткових взаємодій. Температурна залежність ширини резонансної лінії пояснюється моделлю Кубо–Андерсона, час релаксації τ короткий за низьких температур ($\tau \approx 2{,}4 \cdot 10^{-10}$ с) та довгий за високих температур. Зі збільшенням температури *g*-фактор зростає від 1,99 до 2,00, що пов'язано з тепловим розширенням кристалічної ґратки та посиленням спін-орбітальних взаємодій. Інтенсивність сигналу ЕПР зростає зі збільшенням температури, що пов'язано з тим, що зі збільшенням температури більше спінових центрів беруть участь у резонансному процесі, долаючи енергетичний бар'єр. Таким чином, було чітко визначено температурно-залежні магнітні фазові переходи, динаміку спіну та зміну *g*-фактора у монокристалі $MnGaInS_4$. Ці результати вказують на потенціал матеріалу для майбутніх магнітних та спінтронічних застосувань.

Ключові слова: $MnGaInS_4$, ЕПР, *g*-фактор, ширина резонансної лінії, час релаксації.